Published in OPTICAL ENGINEERING / April 1992 / Vol. 31 No.4 / pp. 813 - 825

Objective Image Quality Measure Derived from Digital Image Power Spectra

Norman B. Nill
Brian H. Bouzas
The MITRE Corporation
202 Burlington Rd
Bedford, Massachusetts 01730

Abstract. An objective image quality measure based on the digital image power spectrum of normally acquired arbitrary scenes is developed. This image quality measure, which does not require imaging either designed targets or a constant scene, utilizes the previously known invariance property for the power spectra of arbitrary scenes. The measure incorporates a representation of the human visual system, a novel approach to account for directional differences in perspective (scale) for obliquely acquired scenes, and a filter developed to account for imaging system noise as specifically evidenced in the image power spectra. The primary application is to assess the quality of digital images relevant to the image task of detection, recognition, and identification of man-made objects from softcopy displayed versions of visible spectral region digital aerial images. Experimental verification is presented demonstrating very good correlation (r=0.9) of this objective quality measure with visual quality assessments.

Subject terms: image quality, image assessment, image power spectrum, image processing, image metrics.

Paper 12041 received April 20, 1991; revised manuscript received October 1, 1991;

accepted for publication October 8, 1991.

1 Introduction

It is generally recognized that the most meaningful image quality measures are based on visual (and thus subjective) assessments of images, because in most final uses the images will be viewed by human observers. However, obtaining a sample size of visual image quality assessments large enough to overcome the inherent variability among observers is time-consuming and is often expensive. Thus, objective, rapidly computed image quality measures that correlate acceptably well with perceived image quality are sought, which can substitute for subjective image assessments. Many objective image quality measures have been proposed, developed and used over the years, each with its own set of advantages and disadvantages, and a number of survey papers are available.[1-4]

In this paper we develop an objective, quantitative image quality measure based on the digital image power spectrum of normally acquired arbitrary scenes. Our primary interest is to assess the quality of digital images relevant to the image task of detection, recognition, and identification of man-made objects from softcopy displayed versions of visible spectral region, monochrome, digital, aerial images. The power spectrum approach does not depend on imaging designed targets (such as bars, lines or sinewaves), does not require detection and isolation of naturally occurring targets (such as knife edges), and does not require re-imaging the same scene for comparison purposes (such as via mean square error). This is a major advantage in many operational scenarios where it is highly inconvenient, or simply not possible to insert targets, extract natural targets, or re-image a scene. Essentially, by assuming the invariance (from scene to scene) of the imaging system input scene power spectrum, a measure of the system output image power spectrum denotes the imaging system quality. This image quality measure differs from previous work by applying concepts to the digital image power spectrum domain from human visual perception (visual spatial frequency response characteristics), directional perspective scaling information for oblique images, and a filter to account for noise.

Historically, the genesis for an image quality measure derived from image power spectra is based on research performed over the last 20 years by other researchers, who investigated the shape, form and content of power spectra of arbitrary random scenes. This experimental and theoretical work on scene power spectra was applied, beginning in the 1970s, by researchers who used coherent optical processors to perform the required two-dimensional (2-D) Fourier transform operation on input film imagery.[5,6] The coherent optical processor approach was rapid and demonstrated some success, but it also produced certain artifacts (corruption of the image power spectrum dc by the sampling aperture spectrum and spike noise effects caused by film scratches), and the approach was not readily amenable to isolating individual spectral components for further processing. We began our present research by taking a fresh look at the power spectrum based image quality approach in the digital domain, in light of the fact that more and more imagery today is digital in form; flexible, high speed, compact digital computers are generally available which allow easy incorporation of concepts such as a human vision model; and objective image quality assessment remains as a current problem.

Section 2 of this paper lays the groundwork for the validity of the power spectrum approach for image quality assessment, with a discussion of relevant statistical properties of arbitrary scenes. Section 3 then constructs the power-spectrum-based quality measure by incorporating several beneficial normalizations and derived factors which take into account the human visual system, power spectrum noise, and directional scale information. Section 4 presents experimental results and a discussion thereof, and section 5 summarizes the work accomplished.

2 Scene Power Spectrum Invariance

The foundation of measuring the power spectrum of an image for quality assessment rests on the assumption that the equational form of the imaging system input scene power spectrum is invariant from scene to scene. [As a corollary, the power spectrum is also independent of scale.] This invariance is a necessary assumption for the technique to work when the output image alone is available for measurement. If, in addition to the imaging system performance varying, the input scene power spectrum also varied, it would be impossible to arrive at a measure of image quality whose values could be compared between totally different imaged scenes. On this topic, we note that in a recent paper[7] an image quality measure was presented based on the discrete cosine transform (DCT) of an image. However, since the DCT is unique to each image (i.e., the image can be directly recovered from its DCT), a quality measure based on the DCT can only be relative, i.e., only a comparison between different processed versions of the same image can be made.

At first glance it seems highly unlikely that all scenes have the same power spectrum since, clearly, all scenes are different when viewed in the spatial domain. However, when different scenes are analyzed in the power spectrum spatial frequency domain, wherein all scene phase information is, in effect, irretrievably buried, it can be shown that most arbitrary scenes do indeed theoretically have the same power spectrum. Specifically, the power at the non-zero frequencies goes as $1/\text{frequency}^K$, where K=2 in a one-dimensional (1-D) analysis. In a sense, this constancy should not be too surprising; it probably relates to a fundamental order in natural scenes, which is an area explored in the field of fractal geometry.[8] This inverse frequency power spectrum has been found in a variety of real scenes, including various natural scenes in the visible spectrum[9] and forest scenes in the infrared.[10] It has also been found to be a useful representation for scenes when modeling and optimizing end-to-end imaging system performance.[11]

2.1 Statistical Scene Model

One starting point for the derivation of the invariant scene power spectrum can be found in the theory of statistical point processes, specifically, in what are called *doubly stochastic poisson processes*.[12,13] In a *doubly stochastic poisson process* a stochastic variation in the amplitude of each pulse exists, in addition to the usual poisson process stochastic change/no change event variation. Such a process turns out to be a good model for real, naturally occurring scenes. It was previously applied by Itakura et al [10] and Takagi et al [14] to model the radiance background noise in the infrared spectral region and is applied here to the visible spectral region.

Scanning a scene with a perfect point detector results in a light intensity variation I(x,y), whose magnitude at any given point within the scan is a sample from a random variable and whose probability density function (pdf) can be modeled as a Gaussian, with mean intensity $\bar{I}$ and variance σ_S^2. [Note that a globally constant (stationary) Gaussian intensity behavior is often not observed over an entire real scene, but by assuming a nonstationary mean the gaussian assumption can still be invoked.[15]]

Whether or not there is a *change* in intensity at any given point can be considered an independent random variable with only two event outcomes: either the intensity changes at the point (event 1) or the intensity remains the same as it was at the last point (event 2). Such a two-event random variable has a probability of outcome described by the binomial pdf. In the limit for large sample size and low probability per event, the binomial pdf becomes the Poisson pdf, which in one dimension is,

$$\frac{(a\Delta x)^{\lambda}}{\lambda!}\exp(-a\Delta x), \tag{1}$$

where Δx is the distance interval over which the probability of λ significant changes occur, $a\Delta x$ is the average value of the Poisson process (i.e., the average number of significant changes over the Δx interval), and "a" is the reciprocal of the average pulse width. To bring the scene model postulated into a realistic, physically meaningful realm, a detectable change in intensity is required for event 1 to occur.

We now have a statistical process with two independent random variables and wish to derive the power spectrum representing this process. Assuming stationary statistics and ergodicity, the autocorrelation function can be derived either by taking the expected value between the Gaussian random variable of intensity variation and the Poisson random variable of intensity change, or directly from the spatial average of the pulse process[16].

The Fourier Transform of the 2-D autocorrelation function is (in this case) a rotationally symmetric scene power spectrum, with radial spatial frequency ρ, and constant K,

$$\frac{2\pi a\sigma_s^2}{\left(a^2+\rho^2\right)^{3/2}} + K\bar{I}^2\delta(\rho)\,. \tag{2}$$

Equation 2 represents the power spectrum of an arbitrary 2-D pristine scene input to an imaging system. This pristine scene would, in the case of aerial imaging for example, be uncorrupted by atmospheric haze or turbulence effects; in this application such effects are considered to be part of the imaging system.

3 Construction of an Image Quality Measure from the Image Power Spectrum

3.1 2-D Power Spectrum Definition

Given a 2-D image consisting of M x M pixels, where a pixel's gray level is given by h(x,y) with rectangular spatial coordinates x and y ranging from 0 to M-1, the discrete Fourier transform of the image H(u, v) is defined as

$$H(u,v) = \sum_{x=0}^{M-1}\sum_{y=0}^{M-1}\exp[-2\pi i y\frac{v}{M}]\exp[-2\pi i x\frac{u}{M}]\,h(x,y)\,, \qquad u,v = -\tfrac{M}{2}\bullet\bullet\bullet\tfrac{M}{2}\ . \tag{3}$$

To relate the orthogonal u and v indices of H(u,v) to spatial frequency components of the input image, u and v must be normalized by the number of pixels in the x and y directions, respectively, resulting in u/M and v/M in units of cycles per pixel width (assuming square pixels).

The 2-D image power spectrum of h(x,y) is defined as $|H(u, v)|^2$. Since the input image h(x,y) is an asymmetrical real function, its discrete Fourier transform H(u,v) is hermitian and its power spectrum $|H(u, v)|^2$ is at least bilaterally symmetric with $|H(u, v)|^2 = |H(-u, -v)|^2$. As a result of this symmetry, when computing the image power spectrum one can ignore negative u and v frequencies thereby reducing the amount of data to be processed by a factor of two. An additional factor of two reduction in processing can be obtained by using an FFT implementation which has been optimized for real values of h(x,y).

3.2. Diagnostic Aid: 2-D to 1-D Conversion

Because of the sheer number of data points in the digital 2-D power spectrum and the fact that when plotted it is a surface in three-dimensions, the 2-D power spectrum does not lend itself to easy comparison between images. It is, therefore, useful to generate a 1-D power spectrum which is more tractable and facilitates comparisons between images. We have chosen to generate a form of 1-D power spectrum by averaging the power contained within bands of frequencies, where frequency refers to the radial distance, $\rho = \sqrt{u^2+v^2}/M$, from the origin to the power value at (u,v), in units of cycles per pixel width. We determined that a band width of $\Delta u/M = 1/64$ cycle/pixel width is a good compromise between obtaining a relatively small set of frequency bands while retaining separation of information in the various frequency regions. When the average power in each frequency band is plotted against band center frequency, the curve shape and magnitude track the corresponding quality of the image (except for noisy images) and can help to explain any anomalies. As will be discussed later, the 1-D spectrum can also be used to detect noise, determine the noise variance for white noise, and detect image blur. Note that the image quality measure (IQM) itself, however, is computed from the individual data points of the full 2-D power spectrum.

3.3 Power Spectrum Normalizations

It is necessary to compensate for the effect of image-to-image brightness variations on power spectra magnitudes. This is accomplished by dividing the 2-D power spectrum by μ^2, the square of the average gray level of the image, where $\mu^2 = |H(0,0)|^2/M^4$ and we refer to μ^2 as the dc power. It would be equally valid to normalize the power spectrum by the total power. Brightness normalization was verified by multiplying the gray levels of an 8 bits/pixel image by five different values, representing low to high brightness. The five resulting brightness normalized power spectra all overlapped. The magnitude of the discrete image power spectrum is also proportional to the number of pixels in the input image. Normalization for variation in square image size is accomplished by dividing the 2-D power spectrum by the total number of pixels in the image, M^2.

The combination of brightness and pixel array size normalizations results in a normalized 2-D power spectrum P(u,v) given by

$$P(u, v) = \frac{|H(u, v)|^2}{\mu^2 M^2} . \qquad (4)$$

P(u,v) and image quality measures derived from it can be compared directly for images with different average brightnesses, different size input pixel arrays, and different numbers of bits/pixel. Because several of the quantities to be introduced later are rotationally symmetric, polar coordinates will be used in the remainder of this paper, thus Eq. (4) becomes

$$P(\rho,\theta) = \frac{|H(\rho,\theta)|^2}{\mu^2 M^2}, \qquad \theta = \tan^{-1}\frac{v}{u}. \tag{5}$$

In the special case of wanting to ascertain only the performance of the sensor component of the overall imaging system, it is necessary to normalize out image contrast reduction due to extraneous sources, such as atmospheric haze. This normalization is necessary because uncompensated haze that varies from image to image will lower both visual and power spectrum derived image quality by various amounts, masking the true performance of the sensor, which may in fact be operating in a steady state. It has been shown[17] that contrast reduction due to haze is concentrated in the dc part of the image power spectrum. Therefore, by normalizing $|H(\rho,\theta)|^2$ by the ac component of the power spectrum in place of the previous dc normalization, the haze contrast reduction variable is effectively taken out. This ac normalized power spectrum, $C(\rho,\theta)$, is given by,

$$C(\rho,\theta) = \frac{M^2|H(\rho,\theta)|^2}{\sum_{\theta=-180°}^{180°}\sum_{\rho>0}^{0.5}|H(\rho,\theta)|^2}. \tag{6}$$

Note that ac normalization applied to a hazy image power spectrum can also be used to predict the quality of the equivalent haze-free image that may result from post processing.

3.4 Selection of Image Areas

Because it is only the structured part of an image for which the term "image quality" has meaning, a power-spectrum-based image quality measurement technique requires the selection of image areas which contain structure. Figure 1(a) is an image of San Francisco International Airport and the surrounding area which contains both structure filled city areas and uniform ocean areas. Given an image such as the upper right quadrant of Fig. 1(a), a human will ignore the large uniform ocean area and base a subjective quality rating on the structure along the bottom of the quadrant. Because the power for a uniform area is concentrated in the lower frequencies, the power spectrum and, therefore, any resulting IQM for the upper right quadrant of figure 1a is significantly reduced by the high percentage of relatively constant gray level in the image. [This ocean uniformity is really a result of the degrading effect of the imaging system and low contrast; the inherent spectrum of the ocean maintains the basic inverse frequency shape.]

Figure 1(b) shows the 1-D power spectra for each of the four quadrants of Fig. 1(a) processed independently. The 1-D power spectrum curve for the upper right quadrant is well below those of the other three quadrants. The bottom two quadrants of Fig. 1(a), which consist almost entirely of city elements, show close agreement between their power spectra; the upper left quadrant, which contains both city and ocean areas, falls between the other three quadrants. This case illustrates the importance of avoiding large uniform areas when applying a power-spectrum-based IQM; however this restriction is not severe.

Figure 2(a) and 2(b) illustrate the point that the exact portion of the image selected for processing is not crucial as long as the actual quality is the same throughout the image. Although Fig. 2(a) contains various different objects, the entire image exhibits uniform quality, and there is subsequently only a small variation in 1-D power spectra between various regions of the image, as shown in Fig. 2(b).

(a)

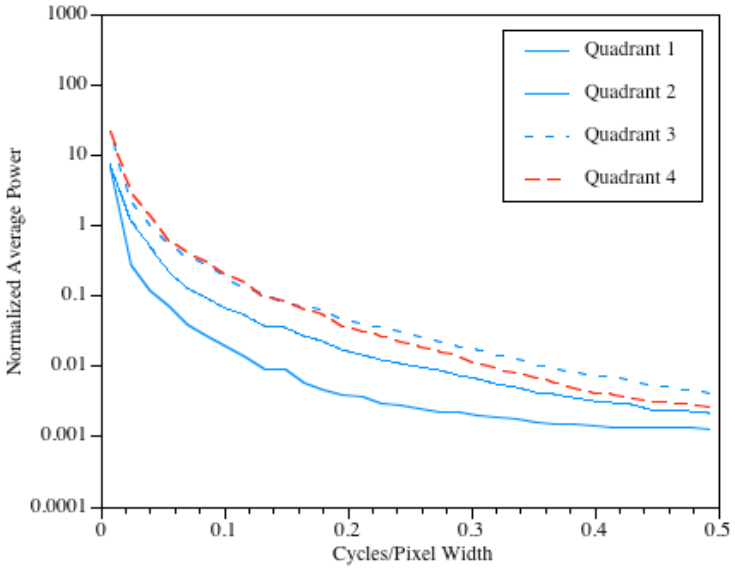

(b)

Fig. 1 Impact of scene structural content on image power spectra. (a) Aerial image of San Francisco international airport. Each quadrant represents a 512 x 512 pixel array. (Grid is not part of image.) (b) Average gray level (and array size) normalized power spectra for each of the 4 scene quadrants; quadrants 2, 3, and 4 have adequate structure while the relatively small area of structure in quadrant 1 is overshadowed by the large uniform ocean area.

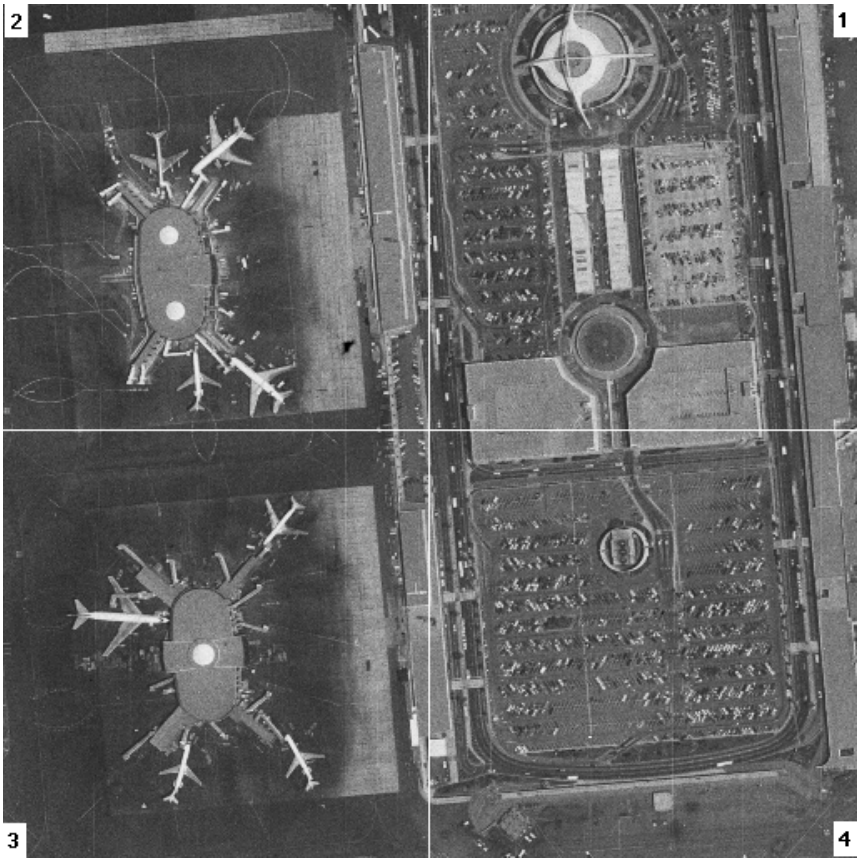

(a)

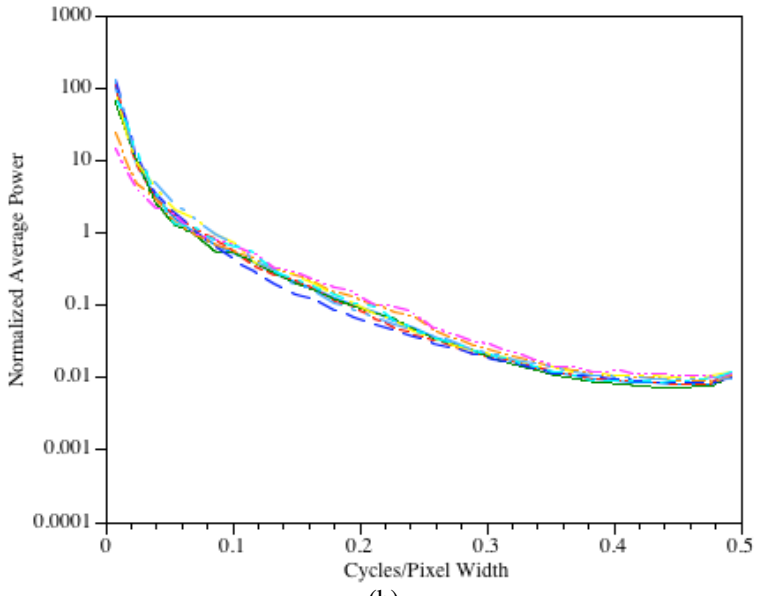

(b)

Fig. 2 Demonstration of scene power spectrum invariance. (a) Aerial image of Los Angeles international airport terminal (grid is not part of image). (b) Average gray level (and array size) normalized power spectra for various independent structure areas (256 x 256 pixel and 512 x 512 pixel segments) and entire 1024 x 1024 pixel image, resulting in only small variation in power spectra.

3.5 Incorporation of Human Visual System (HVS) Model

A number of experimental studies have demonstrated that the inclusion of a model for the human visual system (HVS) in image processing tasks often leads to quantitative results which more closely track the corresponding perceptual response.[18] This has been found in experiments involving objective image quality measures[1,19,20] and in image compression.[21,22] This success with implementing a visual model is in spite of the fact that knowledge of the visual process is incomplete.

Since our end goal is to derive an objective correlate of perceived image quality, we incorporate an HVS model in the power spectrum IQM. The approach is to use the square of a rotationally symmetric modulation transfer function (MTF) representation of the HVS as a filter applied to the image power spectrum. [Squaring the MTF when used with a power spectrum is consistent with linear systems theory.] In our application, an HVS MTF, $A(T\rho)$, is used which was previously constructed[23] as a composite of the psychophysical spatial frequency threshold work of DePalma and Lowry[24] and the experimental trial and error approach of Mannos and Sakrison.[21] Versions of this HVS MTF have demonstrated good results in experimentation on real images.[7, 22] $A(T\rho)$ is shown in Fig. 3 and is defined as

$$A(T\rho) = (0.2 + 0.45T\rho)\exp(-0.18T\rho)\,, \tag{7}$$

where the constant T fixes the spatial frequency of the peak of the HVS MTF with respect to the image's Nyquist frequency and $T\rho$ is in units of cycles/degree subtended by the eye. For unit display magnification, where one digital image pixel maps to one display resolution element, T also fixes the HVS peak with respect to the display's Nyquist frequency. In a comparison of the work of nine independent researchers as reported by Levi[25], a spread exists in the experimentally measured peak location of the HVS MTF ranging from 1 to 9 cycles/degree. The peak of $A(T\rho)$ occurs at 5.11 cycles/degree, which is about the midpoint of this spread.

In relation to the image display, we set this HVS MTF peak location at 20% of the 0.5 cycle/pixel width display Nyquist frequency (hence T = 51.1). This 20% set point was established after consideration of several factors. We are mainly concerned at present with displays of still images viewed for detection, identification and recognition of objects, as opposed to viewing motion images for more general purposes. In the former application, one can reasonably assume that an observer will move far enough away from a display such that the perception of display noise and scan lines are minimized, while at the same time close enough such that essentially all of the information detail presented on the display can be resolved without eyestrain. This allowable variation in observer preferred viewing distance tends to result in the spatial frequency of the peak of the HVS MTF occurring at a constant proportion of the display's Nyquist frequency. It thus makes sense to fix the HVS peak location along the image power spectrum spatial frequency axis to some constant proportion of $\rho = 0.5$ cy/pixel width. Setting the peak location at 20% of Nyquist results in good tracking of the IQM with visual quality assessments, although the exact location of the peak has not been found to be critical.

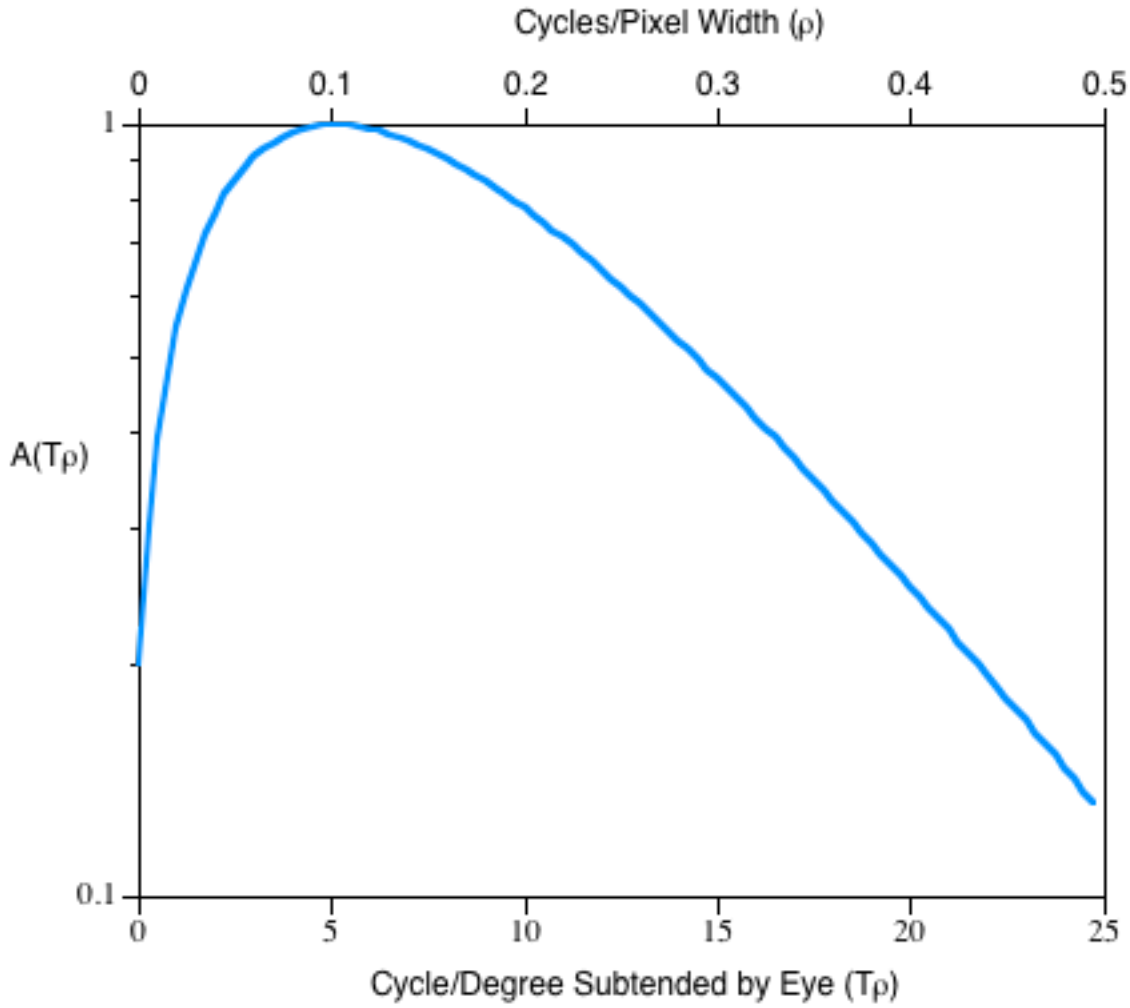

Fig. 3 Rotationally symmetric modulation transfer function representing the human visual system[23] used in the image quality measure. The non-zero frequency peak is attributable to the Mach effect.[37]

3.6 Handling Image System Noise

Noise can become a significant problem in digital imaging systems[26], such as when transmitting a sensor's output image over a noisy channel, when imaging under low light level conditions, or when digitizing film imagery with scan spot sizes on the order of the film grain size. When the common assumption of additive noise in the system is made, the effect on the image power spectrum is as shown in Fig. 4, where the computed power spectrum of an 8 bits/pixel image with and without additive white gaussian noise is given. The noisy image can be represented in one dimension by o(x)+n(x), where o(x) is the output signal and n(x) is the noise. The noisy image power spectrum is then given by $|O(u)|^2+|N(u)|^2+2\text{Real}[O(u)N^*(u)]$, where O(u) and N(u) are the Fourier transforms of o(x) and n(x), respectively, * denotes complex conjugate, and the last two terms in the power spectrum represent the added power. It is apparent from Fig. 4 that any reasonable merit factor applied to the power spectrum (such as area under the curve, moment, etc.) to denote the

corresponding image quality will have a larger magnitude for the noisy image than for the noiseless image. To reverse this trend when noise is present, it is necessary to apply a filter to the computed image power spectrum prior to operating upon it to derive an IQM.

To identify an effective noise filter, a spectral subtraction filter, an empirically derived exponential decay filter, and the Wiener filter were evaluated. The procedure was to add various amounts of white gaussian noise to several digital images, compute the noisy image power spectra with the incorporated noise filter, and assess the resultant 1-D spectrum plots and IQM values.

A modification to the well known Wiener noise filter performed best and is incorporated in the IQM. The classic Wiener filter,[27] here taken to be rotationally symmetric, is given by

$$\frac{|O(\rho)|^2}{|O(\rho)|^2 + |N(\rho)|^2} \quad . \tag{8}$$

In Eq. (8), $|O(\rho)|^2$ is the noiseless image power spectrum, which we represent by the zero mean imaging system input scene power spectrum [term 1 of Eq. (6)] multiplied by the nominal imaging system power spectrum response function (system MTF^2). The system noise power spectrum, $|N(\rho)|^2$, can be obtained in several ways. If the noise is white (flat spectrum) then $|N(\rho)|^2$ simply reduces to the noise variance σ_n^2. We have found that the average power in the Nyquist frequency band (see section 3.2) of the image power spectrum unnormalized by brightness is a very good measure of σ_n^2 for white noise (in the system of units where the pixel dimension is unity),

$$\sigma_n^2 = \frac{\mu^2}{B} \sum_{\theta=-180}^{180} \sum_{\rho=\frac{31}{64}}^{0.5} P(\rho, \theta) \, , \tag{9}$$

where B is the number of data points in the Nyquist band. Other methods of quantifying $|N(\rho)|^2$, particularly useful for colored noise, are to sample a uniform gray level image area, apply a test flash to the sensor, or construct a model of the noise power spectrum shape and then use the actual image Nyquist band value to fix the noise level.

The classic Wiener filter was modified by incorporating one constant (κ_1) that changes the relative weights of the filter components and by another constant (κ_2) that slightly increases the effect of the filter on the image power spectrum:

$$W(\rho) = \left[\frac{2\pi a \sigma_s^2 \exp(-\rho^2/\sigma_g^2)}{2\pi a \sigma_s^2 \exp(-\rho^2/\sigma_g^2) + \kappa_1 (a^2 + \rho^2)^{1.5} |N(\rho)|^2} \right]^{\kappa_2} \tag{10}$$

Table I defines the parameters in Eq. (8) [from which Eq. (10) is derived] and briefly discusses how the parameter values were determined.

The modified Wiener filter can also be used to predict the quality of post-processed noise-filtered images directly from the pre-processed noisy images. This capability is useful for softcopy systems where the quality of the post-processed image is desired, but only an original noisy image is available for power spectrum measurement. An effective noise filter for this case should produce an image power spectrum magnitude that is slightly less than the magnitude of a noiseless-image power spectrum, given that noise filtering results in a small loss of image quality (vis a' vis an

original noiseless image). Equation (10) can be applied to this case by simply using a different value for κ_1 (see Table 1).

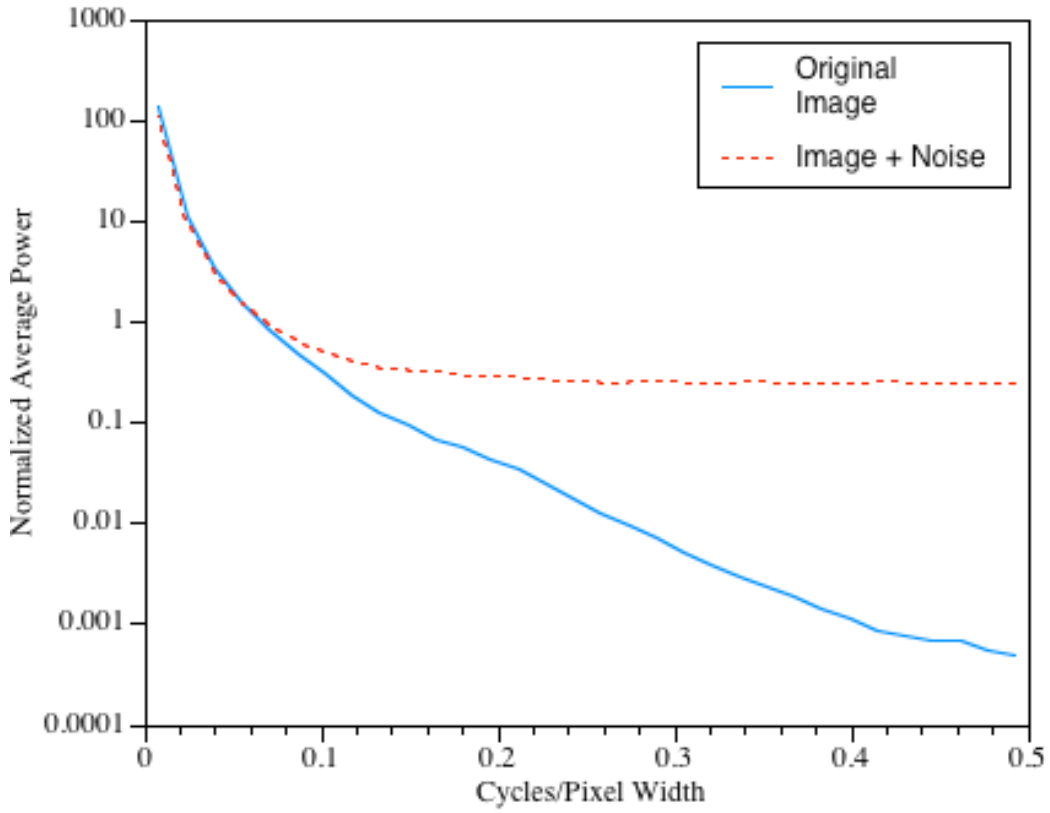

Fig. 4 Impact of system noise on image power spectrum. White gaussian noise (SNR = –1.7 dB) was added to an 8 bit/pixel digital image.

Table 1 Noise filter parameters

$\|O(\rho)\|^2 = [\exp(-\rho^2/2\sigma_g^2)]^2[2\pi a\sigma_s^2)/(a^2+\rho^2)^{3/2}]$ [image system MTF]^2 x [zero – mean scene power spectrum]
$\sigma_g^2 = 0.078$ variance of gaussian MTF with typical 20% modulation at Nyquist
ρ radial spatial frequency in cycles/pixel width
a = 0.926 reciprocal of average pulse width (from measured data)
$\sigma_s^2 = [(0.3125)2^m]^2$ scene variance: typical reflectance variance and mean computed from published data[28] and converted to variance of scene quantized to m bits/pixel
$\kappa_1 = (3355)(2^{-2m})(\sigma_n^2) + 51.2$ (for noisy image) = 19.2 (for post - processed noise filtered image) empirically derived values
κ_2 = 1.5 empirically derived value
$\|N(\rho)\|^2$ noise power spectrum; characterized by σ_n^2 for white noise (see text)

3.7 Directional Scale Factor in IQM

The scene power spectrum is independent of scale, that is, the same equational form is obtained regardless of the scale at which the scene is acquired. However, in many applications image quality is a function of object–image scale. For example, in aerial surveying a scene that is imaged at a scale of 1000:1 would be visually assessed as having higher quality for interpretation of ground objects than the same scene imaged at 10,000:1 scale (assuming constant imaging system performance). For use in such applications, therefore, the image power spectrum is weighted by the ground–image scale.

For vertically acquired aerial images, wherein the optical axis is perpendicular to the ground at nadir, the scale anywhere within the image is constant (for flat terrain) and independent of direction. However, for oblique aerial images, wherein the optical axis is tilted with respect to the vertical, the scale is a function of direction and field location.[29] Given some basic parameters of the image sensor during image acquisition, specifically, sensor look angle α and aircraft altitude above terrain h, the apparent slant range in any direction for an oblique image can be calculated, from which the apparent scale in that direction is easily obtained, given the sensor optics focal length. The appropriate directional scale can then be applied to each individual discrete power spectrum data value, $P(\rho,\theta)$, since directionality information is preserved in going from the image spatial domain to the power spectrum domain. This produces a directional scale weighting factor in the power spectrum IQM which, on conceptual grounds, will more closely track visual quality assessments for aerial images acquired at any view angle. Note that the directional scales are calculated for a single ground location within the image because a single spatial coordinate in the image does not map to a single spatial frequency coordinate in the power spectrum domain (even though directionality is preserved). For this purpose we use the center of the image, where the image is defined by the perimeter of the power spectrum sampling area.

The apparent slant range, D, applicable to a power spectrum data point at angle θ is

$$D = \frac{\left[G^2\cos^2(\beta) + Q^2\sin^2(\beta)\right]^{1/2}}{GQ}. \tag{11}$$

In Eq. (11), G and Q are functions of the true slant range at the field angle component corresponding to the center of the power spectrum sampling area; and β is the angle between the radial line ρ to a specific power spectrum data point $P(\rho,\theta)$ and the sensor look direction (given by the azimuth). G, Q, and all auxiliary quantities are explicitly defined in the derivation of Eq. (11) given in the appendix . Note that once an image location in the sensor's field of view is defined, D only varies with θ.

Scale is incorporated into the IQM by projecting the image pixel size q to the ground, where q is the pixel width, diameter or center-to-center spacing as input to the discrete Fourier transform. The projection uses the apparent slant range D (for oblique images) and the sensor optics focal length f to define the image-to-ground scale. Combining this scale with q results in the IQM parameter $S(\theta_1)$, with spatial frequency units of cycles per ground meter:

$$S(\theta_1) = \frac{f}{2Dq}, \qquad \text{for oblique images}. \tag{12}$$

$$S(\theta_1) = \frac{f}{2hq} , \qquad \text{for vertical images .} \tag{13}$$

$S(\theta_1)$ is multiplied by $P(\rho,\theta)$ in the IQM, analogous to multiplication of the integration interval with the integrand in numerical integration.

3.8 Image Quality Measure

The IQM is derived from the normalized 2-D power spectrum $P(\rho,\theta)$ weighted by the square of the MTF of the human visual system $A^2(T\rho)$, the directional scale of the input image $S(\theta_1)$, and the modified Wiener noise filter $W(\rho)$. The IQM is given by

$$IQM = \frac{1}{M^2} \sum_{\theta=-180°}^{180°} \sum_{\rho=0.01}^{0.5} S(\theta_1)\, W(\rho)\, A^2(T\rho)\, P(\rho,\theta) \quad . \tag{14}$$

The double summation , which reduces the IQM to a single value, is analogous to the 1-D case of taking the area under a weighted system MTF curve to obtain a measure of image quality; the latter has been the basis for many image quality measures.[1,3,4]. The summation also has the benefit of smoothing out directional differences which may occur in some image power spectra caused, for example, by a pattern of parallel streets.

Very low spatial frequency information cannot always be relied upon to be sensitive to quality changes between images. For instance, consider the case of an imaging system having a gaussian MTF. As dramatically large changes in the overall MTF are realized by changing the gaussian's variance by more than an order of magnitude, the percent change in modulation at the very low spatial frequencies is small. We therefore avoid this very low spatial frequency region of the power spectrum by starting the summation for the IQM at 2% of the 0.5 cycle/pixel width image Nyquist frequency. The IQM summation could validly be continued out to the 2-D FFT corner points at ρ=0.707; however, this has only a negligible effect on the IQM magnitude because so little power is beyond ρ=0.5. Division by image size, M^2, is used to normalize the IQM so that there is no weighting by image size. Equation (14) was implemented in FORTRAN on a PC/386 class computer using a real input/complex output Cooley-Tukey FFT algorithm[30] to compute the power spectrum.

4 Performance of the Image Quality Measure

Our primary interest is in objectively assessing image quality relevant to the image task of detection, recognition, and identification of man-made objects from softcopy displayed versions of visible spectral region digital aerial images. To assess the performance of our IQM for this image task, we compare the IQM values measured on a set of digital images to a visual image quality assessment technique which itself is applied to the softcopy displayed versions of the images. Comparison with visual assessments is an important IQM performance verification and validation technique for images which will ultimately be utilized and interpreted by humans. If a strong singular relation is demonstrated, then the objective IQM can replace the subjective visual assessment technique; the latter is often tedious, time-consuming, and labor-intensive.

For this comparison, we use a previously developed and well-established visual image quality scale.[31,32] In this visual scale, a trained image analyst assigns each image a number from 0 to 9 corresponding to the information that he or she can extract when the image is displayed on a well-calibrated, high-quality softcopy display. For example, being able to (only) detect such objects as railroad yards or large aircraft at an airfield would result in an assessed image quality value of 1; being able to identify vehicle types parked in the railroad yard or aircraft types at the airfield would give the image an assessed value of 8.

The power spectrum IQM was applied to a set of fifty digital 8 bit/pixel images for which visual quality assessment values were available. Thirty-three of the images were aerial images of various California urban/suburban areas (San Diego, San Francisco, Los Angeles).[33] These were vertical views acquired in clear weather, originally on film, which was then digitized to 8 bits/pixel monochrome and supplied in either 512 x 512 pixel or 1024 x 1024 pixel segments. These thirty-three images were each assessed on a CRT display by four trained image analysts and the average of the four was used as each image's visual quality value. All but two of the assessed values fell within the visual quality range of 1.0 to 3.0. The other seventeen aerial images represent sparse structure scenes (radio tower/buildings, rural crossroads, bridge/river/forest, etc.) acquired on film at various obliquities up to 60° from nadir. The film was digitized to 512 x 512 pixels, 8 bits/pixel, and each frame was assessed on a CRT display by ten trained image analysts, resulting in average visual quality values ranging from 3.2 to 7.8. For both sets of images the visual assessments were performed on the CRT display without invoking softcopy image enhancements.

The result of applying the IQM of Eq. (14) to the fifty images is shown in a plot of IQM vs average visually assessed quality in Fig. 5. Based on a priori visual assessments of image structural content, the IQM was applied to the full image for approximately half of the images, and in the remaining images, regions of interest no smaller than 256 x 256 pixels were selected. The product moment correlation coefficient, r, between log(IQM) and average image quality is 0.90, which is quite good for a psychophysical experiment. The log of the IQM values are used for this correlation because the values of the visual scale used are related to cycles/ground meter in a logarithmic fashion and our IQM has the dimensions of cycles/ground meter. The importance of making the IQM a function of scale is illustrated by the fact that the correlation with visual quality drops to $r = 0.60$ if the scale factor $S(\theta_1)$ is deleted from the IQM. Since it is the values of the visual scale that have meaning to image analysts, the IQM values are converted to their equivalent visual scale values by using the least squares regression equation given in Fig. 5
.

The performance of the modified Wiener noise filter was verified by selecting 3 of the images with the highest visual quality values and adding small, medium and large amounts of white gaussian noise to each image (SNR values of 9.2 dB, 3.2 dB, and -1.7 dB, respectively). The IQM of Eq. (14) was then applied to each noise corrupted image twice: once with the noise filter parameter κ_1 set for measuring the quality of the noisy image, and once with κ_1 set for predicting the quality of the noise-filtered image (refer to discussion in section 3.6). Figure 6 shows the representative results of applying the modified Wiener filter to the power spectra of one of the three noise corrupted images. The filter correctly decreases the resulting IQM by small amounts for the case of noise-filtered image quality and by large amounts for the noisy image quality case. The values of σ_n^2 as measured from the image power spectra Nyquist band were used in the filter; these values differed from the 3 input gray level noise variances by less than 6 percent on average. The presence or absence of noise can be ascertained from the 1-D image power spectrum by taking the ratio of the power in the $\rho = 0.15$ cy/pixel width frequency band to the power in the Nyquist band. If this ratio is less than five, then noise is present and the noise filter needs to be invoked in the IQM.

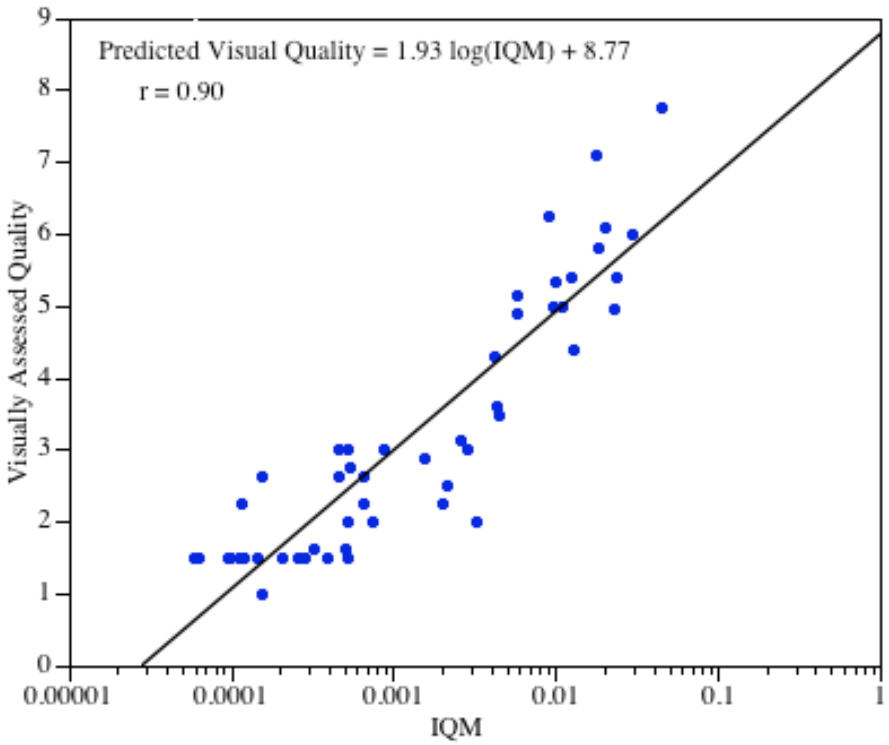

Fig. 5 Overall result of power spectrum image quality measure applied to 50 independent, 8 bit/pixel, aerial, monochrome, visible spectral region images (256^2, 512^2 and 1024^2 pixel images intermixed), compared to average visual quality of each image as assessed by trained observers.

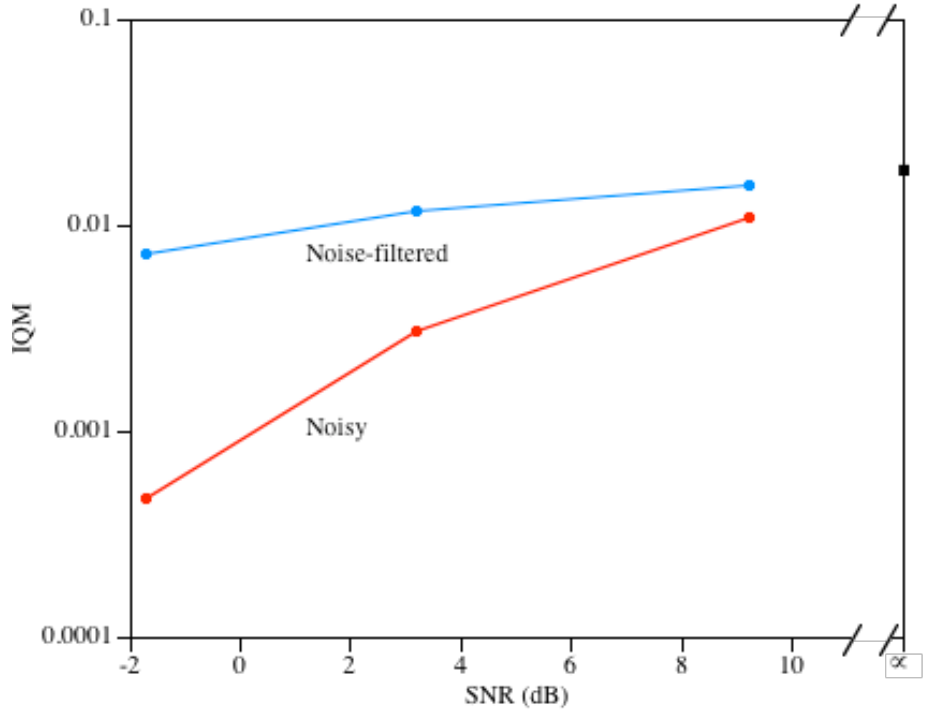

Fig.6 Result of applying modified Wiener noise filter of equation 13 to an image corrupted with noise. Upper curve is with κ_1 set for predicted quality of the noise-filtered image. Lower curve is with κ_1 set for quality of the noisy image.

Pre-processing the input image pixel values, specifically, raising the gray level values to the 0.33 power prior to computing the discrete Fourier transform, has been proposed[18,21,34] as a method of taking into account the nonlinear portion of the HVS. Hanes[35] found some years ago that incident luminance raised to the 0.33 power relates to the perceived brightness of objects, a finding later confirmed by Mansfield.[36] We investigated the use of this pre-processing step with our IQM, but found that it did not aid correlation with visual quality (r remains at 0.90). This outcome could result from a decreased effectiveness of the model when applied to the limited number of image intensity values of digital imagery quantized to 8 bits/pixel (256 gray levels); or the contrast gain of the softcopy display used in assessing the visual quality may have, in effect, already compensated for the nonlinear luminance-perceived brightness relation, negating its utility as a factor in the power spectrum IQM. However, a further investigation determined that incorporation of the linear HVS model, $A^2(T\rho)$, in the IQM also did not aid correlation with visual quality for this set of imagery (r remains at 0.90). We conjecture that an experimentally induced upper bound on the correlation has been reached between the objective IQM and visual assessments for this set of imagery, such that the true merit of an HVS model is masked by this upper bound on r. This upper bound can be attributed to a known variability between the human assessors, as well as some variability between the power spectra of different scenes. In terms of visual assessment variability the standard deviation between observers for some images was as large as 2.0 visual units (average standard deviation across the 50 images is 1.0 visual units). This human variability alone would set a practical upper bound on the correlation coefficient at some value less than 1.0. We are in the process of obtaining a larger image sample size covering a wider range of image types and with less human observer variability; we believe this larger sample size will substantiate the merit of incorporating an HVS model in the IQM.

To further test the IQM performance over the extremes of image quality, the quality of the previous three images (without added noise) was intentionally degraded by (1) adding various amounts of haze and (2) blurring the images. Haze was introduced in accordance with an additive haze model by adding a constant gray level to each pixel in the image and then multiplying all the pixels by a constant value to maintain the same average gray level as the original image. For the case of aerial imagery, haze introduced by atmospheric conditions is an often encountered source of image quality degradation.

As shown in Fig. 7, the IQM does monotonically decrease in magnitude as haze level increases (i.e., as contrast decreases), as would be expected from visual assessments of the imagery. Also shown is the IQM derived from ac normalized power spectra [Eq. (14) with $C(\rho,\theta)$ substituted for $P(\rho,\theta)$], applicable to the special case of isolating sensor performance when haze varies. As desired, the IQM is now constant as haze varies, indicating constant sensor performance.

A general frequency-dependent image degradation ("blur") was introduced by taking the discrete Fourier transform of each of the three images and multiplying the resulting coefficients by a gaussian, $\exp[-\nu^2\rho^2]$, where ν is the blur factor. Figure 8 shows that the IQM decreases as the blur increases, as it should. However, a visual assessment of the blurred images indicated that they had lower visual quality than was computed by the IQM. An analysis of the corresponding 1-D power spectra indicated that the spatial frequency region of quality sensitivity shifts to higher frequencies for blurred images. Therefore, by deleting the lower frequency information used in the IQM, the IQM regains good tracking with visual quality for the blurred images, as shown in Fig.8. Specifically, the lower limit of summation in the IQM was changed from 2% of Nyquist to 20% of Nyquist.

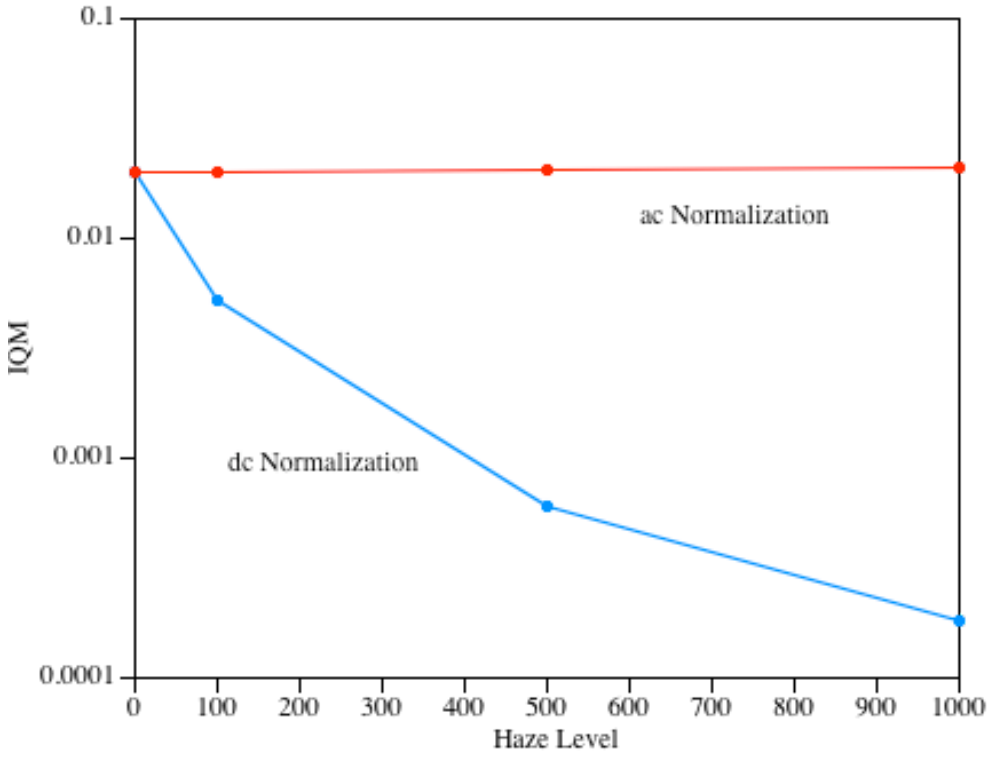

Fig. 7 Effect of image contrast reduction (simulated atmospheric haze) on IQM derived from dc normalized power spectrum and from ac normalized power spectrum. The curve for ac normalization has a scaling constant to bring its magnitude within the range of the curve for dc normalization.

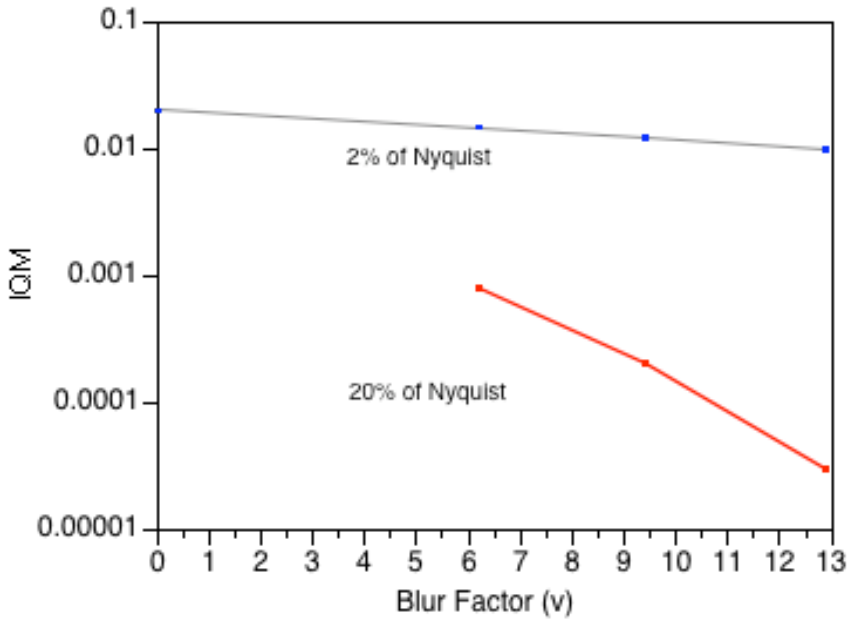

Fig. 8 IQM results for blurred imagery. Power summation for IQM starts at 2 % of Nyquist in upper curve and 20% of Nyquist in lower curve.

A test can be applied to the power spectrum to detect the presence of frequency dependent degradation and, if present, the lower limit of summation in the IQM can be automatically shifted to the higher frequency. From Fourier theory it is known that the rate at which the power spectrum dies away is directly proportional to the smoothness of its transform (the autocorrelation function), and increasing frequency dependent degradation of the image results in a smoother autocorrelation. This Fourier property can be used to determine the presence of blur by measuring the rate of decrease of the power spectrum. We can apply this concept, tailored to the specific problem, by determining the average rate of change of the 1-D log power versus frequency relation over a telltale frequency range, which appears to be from 10% to 50% of the Nyquist frequency. The result of applying this concept to all of the images indicates that the procedure works. Specifically, for the 50 original, non-blurred images, the 9 added haze images, and the 9 added-noise images, the average /slope/ over the 10% to 50% Nyquist frequency region is always less than 12 (average= 7.9), whereas for the 9 blurred images the average slope is always greater than 13 (average = 17.1). This indicates a clear demarcation between blurred and non-blurred images.

5 Summary

We have developed an objective image quality measure based on digital image power spectra. Good correlation of this measure with visual quality of aerial images assessed for their informative value (detection, recognition and identification of man-made objects) has been demonstrated. The quality measure incorporates a modulation transfer function representation of the human visual system. As the science of vision research advances, it is expected that the visual system response model can be refined and combined with a model of softcopy display image quality characteristics. A novel approach was utilized for handling obliquely acquired scenes by defining (and deriving) a directional scale factor for inclusion in the quality measure. For application to those cases where digital image noise exists, a modified Wiener filter, adaptive to specific noise situations, was constructed and incorporated into the quality measure. It was shown that a simple test applied to the image power spectrum can determine the presence of noise and that the variance of white noise can be accurately and easily estimated from the power spectrum.

A major benefit of an image quality measure based on image power spectra is that it is applied to the naturally imaged scene as is. It does not require use of designed quality assessment targets or re-imaging the same scene for comparison purposes; it requires only a selection of an image area containing some structure. Although the required 2-D discrete Fourier transform operation is computationally intensive, current digital hardware overcomes this difficulty, allowing potentially wide application of this quality measure.

6 Appendix: Directional Apparent Slant Range for Oblique Images

If we refer to Fig. 9 and assume that the ground elevation at the image location p_3 equals the ground elevation at nadir, p_5, then the true slant range L_0 along the optical axis p_2p_3 and corresponding to sensor look angle α is (from law of cosines)

$$L_0 = \left[E^2 + (E+h)^2 - 2E(E+h)\cos\varphi_\alpha \right]^{1/2} . \tag{15}$$

In many cases the sensor look angle must be determined from its given component tilt angle τ and given component side pointing angle χ. Tilt refers to the component of the optical axis with respect to nadir line p_2p_5 in the flight line plane, and the side pointing angle refers to the

component of the optical axis with respect to the nadir line in a plane 90° to the flight line. The sensor look angle is then determined from plane triangle $p_1p_2p_3$:

$$\alpha = \sin^{-1}\left(\frac{E\sin\varphi_\alpha}{L_0}\right), \tag{16}$$

where $\varphi_\alpha = b/E$ and arc length b is defined from the right spherical triangle $P_5P_4P_3$ as

$$b = E\cos^{-1}\left(\cos\varphi_{|\tau|}\cos\varphi_{|\chi|}\right). \tag{17}$$

[The projection of b onto the image plane is the principal line.]

Since the full gamut of L values are completely defined over just one quadrant the magnitude of τ and χ can be used, thereby avoiding the need for taking into account any given sign convention and resulting in the convenient limits: $0 \le |\tau| < \pi/2$, $0 \le |\chi| < \pi/2$.

Now substituting b/E for φ_α in Eq. (16) and using the relation $\sin[\cos^{-1}(x)] = (1\text{-}x^2)^{1/2}$ gives

$$\alpha = \sin^{-1}\left[\frac{E}{L_0}\left(1 - \cos^2\varphi_{|\tau|}\cos^2\varphi_{|\chi|}\right)^{1/2}\right], \tag{18}$$

where

$$\varphi_{|\tau|} = \sin^{-1}\left(\frac{E+h}{E}\sin|\tau|\right) - |\tau|, \tag{19}$$

and

$$\varphi_{|\chi|} = \sin^{-1}\left(\frac{E+h}{E}\sin|\chi|\right) - |\chi|. \tag{20}$$

Similarly, the azimuth angle ψ is determined from right spherical triangle $p_5p_4p_3$:

$$\psi = \sin^{-1}\left[\frac{\sin\varphi_{|\tau|}}{\left(1 - \cos^2\varphi_{|\tau|}\cos^2\varphi_{|\chi|}\right)^{1/2}}\right]. \tag{21}$$

It is convenient (with no loss of correctness) to consider the image–ground slant range as having an effective or apparent value, the value depending on orientation. In a direction perpendicular to b, i.e., along a line parallel to the true horizon, the apparent slant range is equal to the true slant range L_ε. But along a line collinear with b, the apparent slant range is

$$\frac{L_\varepsilon\cos\varepsilon}{\cos(\alpha - \varepsilon)}, \tag{22}$$

where ε is the component of the sensor optics field angle along b. ε is positive on the nadir side of the optical axis and negative on the horizon side. [The term cos ε/cos(α−ε) in Eq. (22) is equivalent to the width of a ground object taken along the b line divided by the width projected onto a perpendicular to the optical axis. For example, see Moffitt,[29] pg 407, and work out WU/WU'.] L_ε can be found by substituting $\phi_{\alpha-\varepsilon}$ for ϕ_α in Eq. (15), where $\phi_{\alpha-\varepsilon}$ is computed by substituting $(\alpha-\varepsilon)$ for $|\tau|$ in Eq. (19). Note that for low sensor altitudes (below 1500 meters) it is computationally more tractable to utilize the simpler flat earth model to compute L_o, L_e, α, and ψ from plane geometry.

Equation (22) and L_ε determine the apparent slant ranges in orthogonal directions at any point on the principal line. The apparent slant range in any intermediate direction can be approximated by use of properties of an ellipse. That is, if an array of small circles is photographed with an oblique camera (each circle covering a very small field angle), then an array of ellipses results in the image plane, where L_ε and Eq. (22) are inversely proportional to the major and minor axes of any ellipse occurring on the principle line. At any point on the principal line, therefore, the apparent slant range D in any direction can be closely approximated by utilizing the reciprocal of the polar form equation of an ellipse,

$$D = \frac{\left(G^2\cos^2\beta + Q^2\sin^2\beta\right)^{1/2}}{GQ}, \tag{23}$$

where G is 1/2 the minor axis length, which is equal to $1/L_\varepsilon$ for the case of L_ε greater than Eq. (22), and Q is 1/2 the major axis length, which is equal to the reciprocal of Eq. (22) for the same case. For the case of L_ε less than Eq. (22), G equals the reciprocal of Eq. (22), and Q equals $1/L_\varepsilon$.

The angle β relates each image power spectrum data point $P(r,\theta)$ to the corresponding directional slant range. From Fig. 10 we obtain

$$\beta = \gamma + \theta_1 - \psi, \tag{24}$$

where γ is the magnitude of the angle between the pixel sampling array positive x axis and the ground projection of the sensor aircraft crosstrack line (positive x axis defined to be between positive flight line axis and positive crosstrack line axis). Since the image power spectrum is bilaterally symmetric, power values are actually only computed over the two quadrants (+u,+v) and (+u,-v), where the x,y image axes correspond to the u,v power spectrum axes, respectively. However, since D is completely defined over just one quadrant (+u,+v), $0 \le \psi \le \pi/2$, and θ_1 is taken to be the equivalent value of θ in the (+u,+v) quadrant, $\theta_1 = \tan^{-1}(|v|/|u|)$.

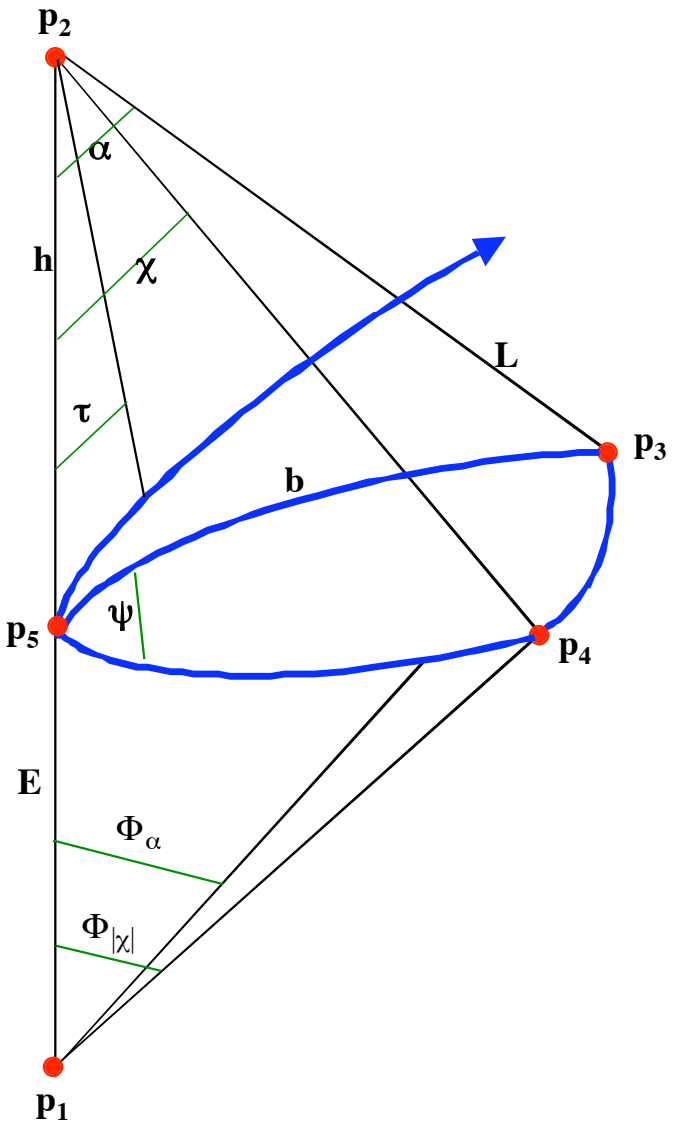

Fig. 9 Geometry for derivation of apparent directional slant range: sensor aircraft at p_2 at altitude h above terrain, ground image located at p_3, and center of earth at p_1. Heavy lines lie on earth's surface; arrow line is flight direction projected to ground; p_5p_4 is crosstrack line.

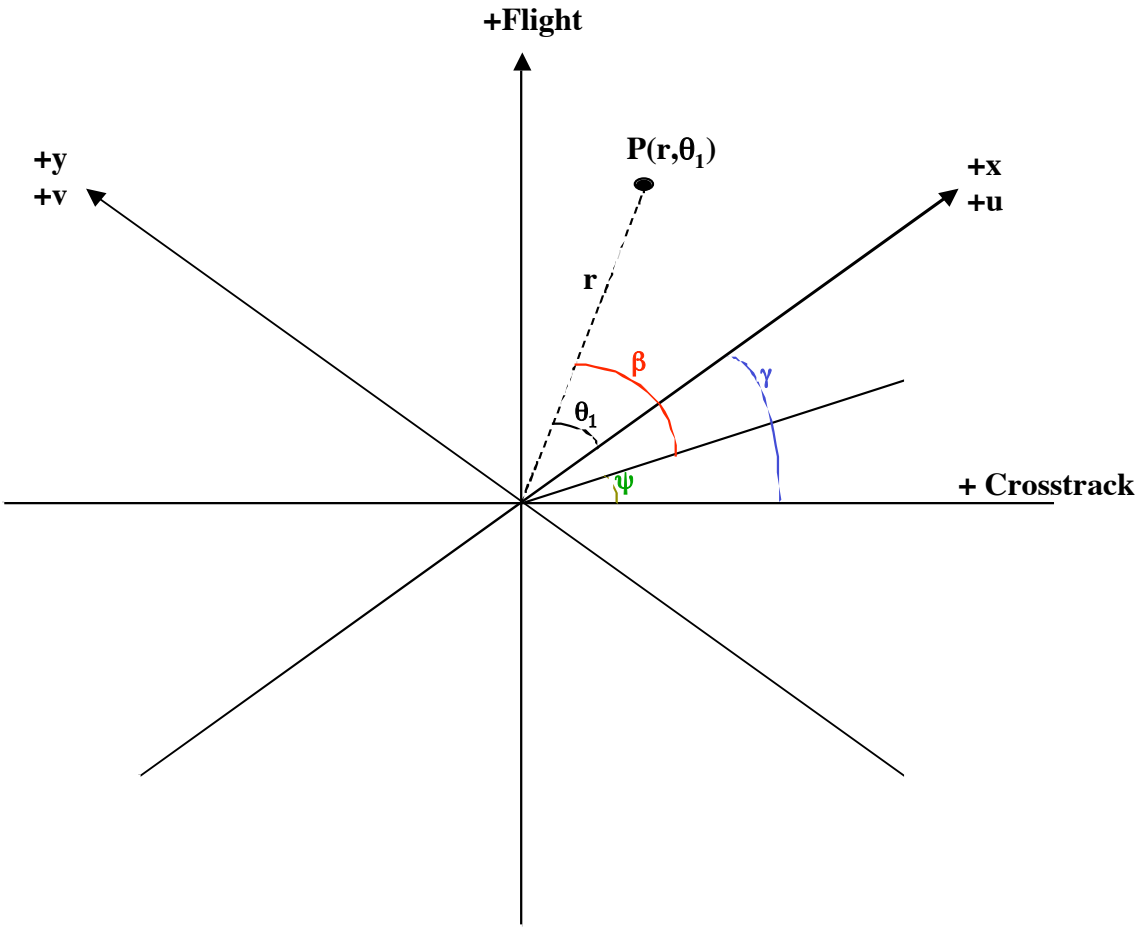

Fig. 10 Orientation convention for relating a given digital image power spectrum data point, P(r,θ), with the appropriate apparent slant range direction angle, β.

Acknowledgements

This research was supported by the Electronic Systems Division of the United States Air Force, under contract F19628-89-C-0001.

References

1. G. C. Higgins, "Image quality criteria," J. Appl. Photgr. Eng. **3 (2)**, 53-60 (1977).

2. O. H. Schade, "Image quality - a comparison of photographic and television systems," SMPTE J.**96(6)**, 567-648 (1987).

3. H. L. Snyder, "Image quality: measures and visual performance," in *Flat Panel Displays and CRTs*, L. E. Tannas (Jr.), ed, Van Nostrand Reinhold, New York, (1985), pp. 70-90.

4. W. L. Wetherell, "The calculation of image quality," in *Applied Optics and Optical Engineering*, **8**, R. R. Shannon and J. C. Wyant, eds. Academic Press, New York, (1980), pp. 172-316.

5. N. B. Nill, "Scene power spectra: the moment as an image quality merit factor," Appl. Opt. **15 (11)** 2846-2854 (1976).

6. A series of nine papers (authors: P.T. Gough and B.J. Thompson, R.R. Shannon, N. Balasubramanian and H. J. Liff, R. A. Schindler, S. A. Armstrong and B. J. Thompson, H. L. Kasden, G. E. Lukes, N. Balasubramanian, and R. D. Leighty) in *Data Extraction and Classification From Film*, Proc. SPIE **117**, 1-132 (1977).

7. J. A. Saghri, P. S. Cheatham, and A. Habibi, "Image quality measure based on a human visual system model," Opt. Eng. **28 (7)**, 813-818 (1989).

8. K. Falconer, *Fractal Geometry - Mathematical Foundations and Applications* , Wiley, New York (1990).

9. D. J. Field, "Relations between the statistics of natural images and the response properties of cortical cells," J. Opt. Soc. Am.A. **4 (12)** 2379-2394 (1987).

10. Y. Itakura, S. Tsutsumi, and T. Takagi, "Statistical properties of the background noise for the atmospheric windows in the intermediate infrared region," Infrared Physics **14**, 17-29 (1974).

11. F. O. Huck, C. L. Fales, J. A. McCormick, and S. K. Park, "Image-gathering system design for information and fidelity," J. Opt. Soc. Am.A. **5 (3)** 285-299 (1988); and --, "Wiener restoration of sampled image data: end-to-end analysis," J. Opt. Soc. Am. A.5 (3), 300-314 (1988).

12. J. Grandell, *Doubly Stochastic Poisson Processes*, Springer-Verlag, New York (1976).

13. D. L. Snyder, *Random Point Processes* , Wiley, New York (1975).

14. T. Takagi and S. Tutumi, "Statistical properties of radiance spatial distribution of sky and forest backgrounds", J. Electronics and Communications in Japan, **51-C (2)**, 82-90 (1968).

15. B. R. Hunt and T. M. Cannon, "Nonstationary assumptions for gaussian models of images," IEEE Trans. Syst., Man, Cybern. **SMC-6 (12)**, 876-882 (1976).

16. C. W. Helstrom, *Statistical Theory of Signal Detection,* Pergamon Press, New York (1968).

17. N. B. Nill, "Contrast effect on imagery power spectra," Appl. Opt. **18**, **(13)** 2147-2151, (1979); and errata: N. B. Nill, Appl. Opt. **19 (24)** 4135 (1980).

18. D. J. Granrath, "The role of human visual models in image processing," Proc. IEEE **69 (5)** 552-561, (1981).

19. R. J. Beaton, R. W. Monty, and H.L. Snyder, "An evaluation of system quality metrics for hard-copy and soft-copy displays of digital imagery," in *Applications of Digital Image Processing VI*, Proc. SPIE **432**, 320-328 (1983).

20. F. X. J. Lukas and Z. L. Budrikis, "Picture quality prediction based on a visual model," IEEE Trans. Commun. **COM-30 (7)**, 1679-1692 (1982).

21. J. L. Mannos and D. J. Sakrison, "The effects of a visual fidelity criterion on the encoding of images," IEEE Trans. Inform. Theory **IT-20 (4)**, 525-536 (1974).

22. K. N. Ngan, K. S. Leong, and H. Singh, "Adaptive cosine transform coding of images in perceptual domain," IEEE Trans. Acoust. Speech Signal Process. **ASSP-37 (11)**, 1743-1750 (1989).

23. N. B. Nill, "A visual model weighted cosine transform for image compression and quality assessment," IEEE Trans. Commun. **COM-33 (6)**, 551-557 (1985).

24. J. J. DePalma and E. M. Lowry, "Sine wave response of the visual system. II. Sine wave and square wave contrast sensitivity," J. Opt. Soc. Am. **52 (3)**, 328-335 (1962).

25. L. Levi, "Vision in communication," in *Progress in Optics*, **8**, E. Wolf, ed, American Elsevier, New York (1970), pg. 358.

26. T. E. Jenkins, *Optical Sensing Techniques and Signal Processing* , Prentice Hall, Englewood Cliffs, NJ (1987).

27. J. S. Lim, *Two-dimensional Signal and Image Processing* , Prentice Hall, Englewood Cliffs, NJ (1990), pp. 527-546.

28. AFCRL, *Handbook of Geophysics* , MacMillan, New York (1960), pg. 14-4.

29. F. H. Moffitt, *Photogrammetry* , International Textbook, Scranton, PA, 2nd edition (1967).

30. F. T. Krogh, "RFT-multidimensional real Fourier Transform," Jet Propulsion Lab Technology Utilization Document CP-2309, Pasadena, CA (1970); source code available from NASA/COSMIC, 382 E. Broad St., Athens, GA 30602.

31. H. L. Snyder, "Quality metrics of digitally derived imagery and their relation to interpreter performance: VIII (interim report)," Virginia Polytechnic Institute and State University Tech. Rep. HFL-83-1, Blacksburg, VA (1983).

32. L. Scarff, "EO imaging system performance prediction and measurement," in *Conference Summaries, 43rd Annual Conference of SPSE,* Society of Imaging Science and Technology, 234-237 (1990).

33. A. Weber, "The USC image processing institute database," University of Southern California Tech. Rep. USCIPI-1060, Los Angeles, CA (1981).

34. C. F. Hall and E. L. Hall, "A nonlinear model for the spatial characteristics of the human visual system," IEEE Trans. Syst., Man, Cybern. **SMC-7 (3)**, 161-170 (1977).

35. R. M. Hanes, "The construction of subjective brightness scales from fractionation data: a validation," J. Experimental Psychology **39**, 719-728 (1949).

36. R. J. W. Mansfield, "Visual adaptation: retinal transduction, brightness and sensitivity," Vision Research. **16**, 679-690 (1976).

37. F. Ratliff, *Mach Bands: Quantitative Studies on Neural Networks in the Retina* , Holden-Day, San Francisco, (1965).